



# SIMULATION OF RESIN INFUSION PROCESSES

**Piaras A. Kelly, Carl J. Johnson, Don A. Nield**  
**Department of Engineering Science, The University of Auckland**

**Keywords:** *simulation, finite element method, resin infusion, VARTM*

## Abstract

*This study is concerned with Resin Infusion Liquid Composite Molding processes such as Vacuum Assisted Resin Transfer Molding. The Resin Infusion process has been effectively simulated using two models, one based on the conventional Darcy's Law and one based on a height-averaged modified version of Darcy's Law.*

*The finite elements themselves are used as control volumes and a mass conservation technique is applied to improve the accuracy of fluid flux evaluation. Elements at the flow front are temporarily subdivided to allow for convergence of the numerical scheme.*

*It is found that the temporal height derivative is important and cannot be neglected if one is interested in an accurate simulation. Neglecting this term to form the quasi-static forms of the full governing equations significantly increases the mass balance error and can greatly reduce the mold fill time.*

## 1 Introduction

Liquid Composite Molding (LCM) processes are a family of advanced composite material manufacturing processes, gaining popularity in the aerospace, automotive and military industries. They include the hard-mold Resin Transfer Molding (RTM) and Injection/Compression Molding (I/CM) processes. One of the appeals of these processes is that, with their closed molds, harmful emissions are minimized. This study is concerned with the Resin Infusion flexible bag LCM processes such as Vacuum Assisted Resin Transfer Molding (VARTM). Here, a vacuum is generated within the mold and resin infuses in under pressure. The external pressure can be applied to the flexible bag in a number of ways, for example through atmospheric pressure or due to contact with a pressurized fluid. These Resin Infusion processes,

with their relatively inexpensive molds, facilitate the production of large and complex geometries.

There is a need for simulation of the infusion process as prototyping is expensive and control of the final thickness is important. The most common computational method of simulating LCM processes is the Control-Volume Finite Element Method which has been developed and tested extensively on RTM processes [1] and, to a lesser extent, for other LCM processes (e.g. [2]). An attractive alternative method is one which uses non-conforming finite elements with a special modification to ensure mass conservation on the element level [3]. The finite elements play the part of the control volumes, thus simplifying domain discretisation and resin flow calculations at the flow front. This method has been shown to be well suited to the I/CM process, in which thickness changes occur during the filling stage [3]. In this paper, the method is extended to deal with the more complex infusion processes.

The thickness variation along the preform during filling plays an important role in this study. As such, what follows is most appropriate to Resin Infusion processes in the absence of distribution media, since thickness variations are not so prominent with such media.

## 2 Formulation

### 2.1 Governing Equations

The continuity equation appropriate for a thickness-varying planar LCM process is

$$\nabla \cdot (h\mathbf{q}) = -\frac{\partial(\phi h)}{\partial t}, \quad (1)$$

where  $h$  is the thickness of the component,  $\phi$  the porosity and  $\mathbf{q}$  the Darcy velocity. With conservation of fibre mass,  $V_f h = \text{constant}$ ,  $V_f$  being the fibre volume fraction, one has

$$\nabla \cdot (h\mathbf{q}) = -\frac{\partial h}{\partial t}. \quad (2)$$

The Darcy velocity is related to the fluid pressure  $p$  through Darcy's law:

$$\mathbf{q} = -\frac{\mathbf{K}}{\mu} \nabla p, \quad (3)$$

where  $\mathbf{K}$  is the permeability tensor and  $\mu$  is the fluid viscosity.

Combining (2) and (3) leads to the governing LCM equation

$$\nabla \cdot \left( h \frac{\mathbf{K}}{\mu} \nabla p \right) = \frac{\partial h}{\partial t}. \quad (4)$$

In this equation, the thickness  $h$ , pressure  $p$  and permeability  $\mathbf{K}$  are coupled. The thickness and permeability are related by an empirical equation of the form

$$K_{ij} = K_{ij}(h), \quad (5)$$

for example the Carman-Kozeny relation.

The fluid pressure is related to the stress  $\sigma_f$  taken up by the fibrous preform and the (known) externally applied stress  $\sigma_{ext}$  through Terzaghi's relation,

$$\sigma_f + p = \sigma_{ext}. \quad (6)$$

In the infusion process, this external stress will usually be constant, for example the atmospheric pressure  $p_{atm}$ . The fibre stress and thickness are related by a constitutive law for the fibrous material,

$$\sigma_f = \sigma_f(h), \quad (7)$$

which is usually taken to be a non-linear elastic law, but can also express the viscoelastic properties of fibrous materials. This expression incorporates the differences which occur when the preform is dry and when it is saturated – in the latter case giving lower stress values for a given thickness.

## 2.2 Height Averaged Darcy Law

Eqn. 3 is the standard form for Darcy's law. However, in planar flows with thickness variations it could be argued that it is more appropriate to use a

height-averaged form of Darcy's law, which takes the height variation in any representative volume element into account:

$$\mathbf{q} = -\frac{\mathbf{K}}{\mu} \frac{1}{h} \nabla(ph). \quad (8)$$

Some justification for this modification can be obtained from open-channel flow laws where, for example, force balance results in similar gradient terms as on the right hand side of Eqn. 8.

The governing equation analogous to Eqn. 4 in this case is

$$\nabla \cdot \left( \frac{\mathbf{K}}{\mu} \nabla(ph) \right) = \frac{\partial h}{\partial t}. \quad (9)$$

Both versions of Darcy's law will be used in what follows; the standard version will be denoted by "SD" and the height-averaged version will be denoted by "AD".

## 2.3 Galerkin Finite Element Method

Using the standard Galerkin Finite Element Method (GFEM), multiplying Eqn. 4 by a weight function  $\omega$  and integrating over the fluid-filled region leads to

$$\int_s \left( \nabla \cdot \left( h \frac{\mathbf{K}}{\mu} \nabla p \right) \right) \omega dS = \int_s \frac{\partial h}{\partial t} \omega dS, \quad (10)$$

and an application of Green's theorem leads to the weak form

$$\begin{aligned} & \int_s \left( h \frac{\mathbf{K}}{\mu} \nabla p \right) \cdot \nabla \omega dS \\ &= \int_c \omega \left( h \frac{\mathbf{K}}{\mu} \nabla p \right) \cdot \mathbf{n} dC - \int_s \frac{\partial h}{\partial t} \omega dS \end{aligned} \quad (11)$$

The (AD) weak form of Eqn. 9 is obtained in the same way.

Discretising the three variables  $h$ ,  $p$ ,  $\mathbf{K}$ , with appropriate shape functions, e.g.,  $p(x) = \sum p_i N_i(\mathbf{x})$ , and evaluating the integrals over each element, which now involve the shape functions only, leads to a set of non-linear equations of the form

$$\mathbf{K}_{ST}(\mathbf{h}) + \mathbf{C} \frac{\partial \mathbf{h}}{\partial t} = \mathbf{F}(\mathbf{h}), \quad (12)$$

where  $\mathbf{h}$  is a vector of nodal heights and  $\mathbf{K}_{ST}$ ,  $\mathbf{C}$ ,  $\mathbf{F}$  are, respectively, elemental stiffness, capacitance and flux vectors.

Using a forward finite difference approximation for the height derivative, the resulting GFEM equations can be solved explicitly. However, in order to avoid instabilities and the necessity of ever-refining the mesh for convergence, it is necessary to solve the equations implicitly, using a backward difference approximation

$$\frac{\partial h}{\partial t} \approx \frac{h^t - h^{t-\Delta t}}{\Delta t}. \quad (13)$$

A Newton-Raphson approach can now be employed to solve Eq. 12. In this case, in the construction of the elemental tangent matrix,  $\partial \mathbf{K}_{ST} / \partial \mathbf{h}$ , the derivatives of the functions in Eqns. 5 and 7 are required.

## 2.4 Conserved Mass Flux Evaluation

The governing equations can be solved for  $h$  and hence  $\mathbf{K}$  and  $p$  using, for example, linear triangular elements. The flux  $\mathbf{q}$  can then be evaluated from Darcy's law, Eqn. 3 (SD) or 8 (AD). With linear elements this leads to a constant flux  $\mathbf{q}_{FE}$  over each element. An improved linear approximation  $\mathbf{q}_a$  can be achieved by using a Taylor series expansion about the barycentre  $\mathbf{x}_B$  of the element,

$$\mathbf{q}_a(\mathbf{x}) = \mathbf{q}_a(\mathbf{x}_B) + \nabla \mathbf{q} \Big|_{\mathbf{x}=\mathbf{x}_B} (\mathbf{x} - \mathbf{x}_B). \quad (14)$$

One of the principle motivations for this approach is that it dispenses with the need for control volumes, allowing for accurate flux evaluation on the element level, by incorporating conservation of mass, particularly with non-conforming elements [4].

Assume that the flux behaves as for the lowest-order Raviart-Thomas element,

$$\mathbf{q}_a(\mathbf{x}) = \begin{bmatrix} r + sx \\ t + sy \end{bmatrix}, \quad (15)$$

which ensures that, for each element edge, the normal flux is constant. It follows that

$$\frac{\partial \mathbf{q}}{\partial \mathbf{x}} \Big|_{\mathbf{x}=\mathbf{x}_B} (\mathbf{x} - \mathbf{x}_B) = \frac{1}{2} (\nabla \cdot \mathbf{q}_a) (\mathbf{x} - \mathbf{x}_B). \quad (16)$$

Using the relation

$$\nabla \cdot (h\mathbf{q}) = h\nabla \cdot \mathbf{q} + \nabla h \cdot \mathbf{q}, \quad (17)$$

and locally ensuring conservation of fluid mass through Eqn. 2, one has

$$\begin{aligned} \mathbf{q}_a(\mathbf{x}) = \mathbf{q}_a(\mathbf{x}_B) - \frac{1}{2} \frac{1}{h} \frac{\partial h}{\partial t} \Big|_{\mathbf{x}_B} (\mathbf{x} - \mathbf{x}_B) \\ - \frac{1}{2} \frac{1}{h} \nabla h \cdot \mathbf{q}_a \Big|_{\mathbf{x}_B} (\mathbf{x} - \mathbf{x}_B) \end{aligned} \quad (18)$$

The quantity  $\mathbf{q}_a(\mathbf{x}_B)$  here can be taken to be the finite element (constant) solution for flux,  $\mathbf{q}_{FE}$ . The second and third terms on the right hand side of Eqn. 18 are relatively inexpensive to evaluate and can be viewed as ‘‘post-processing’’ correction terms to the direct finite element solution.

Eqn. 18 applies to both the standard (SD) and height-averaged (AD) Darcy's law, with  $\mathbf{q}_{FE}$  evaluated, respectively, using Eqn. 3 and Eqn. 8.

## 3 Solution Method

### 3.1 Flow front conditions

Fig. 1 shows a typical perform cross-section at the flow-front. Ahead of the flow front the preform is dry and maintains its equilibrium thickness, point  $c$ . Behind the flow front the preform is wet, point  $a$ . For a given fibre stress, the thickness at  $a$  will be less than at  $c$ , due to the wet/dry difference. Competing with this is the additional fluid pressure behind the flow front which tends to increase the thickness there (see Eqn. 6). Any zone of partial saturation which might pertain between  $a$  and  $c$  is discounted and a sharp flow front is assumed, at  $b$ .

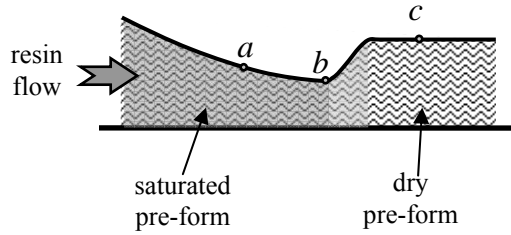


Fig. 1. Typical perform profile at the flow-front

### 3.2 Solution Procedure

One fixed grid of elements is generated at the start of the simulation. The initial conditions are obtained using the quasi-static approximation  $\partial h / \partial t = 0$ , giving the height profile in the initially saturated region. With the height known, the pressure and permeability can be evaluated through Eqns. 5-7. The flow-front is then advanced using the Darcy velocity calculated from Eqn. 18. Temporary nodes are positioned at the new flow-front thus obtained. This is achieved by subdividing elements at the flow front into sub-elements, for example a triangular element into four sub-triangles (see, for example, [5]). The thickness at these temporary flow-front nodes is set to that corresponding to a wet perform with zero fluid pressure, Fig. 2.

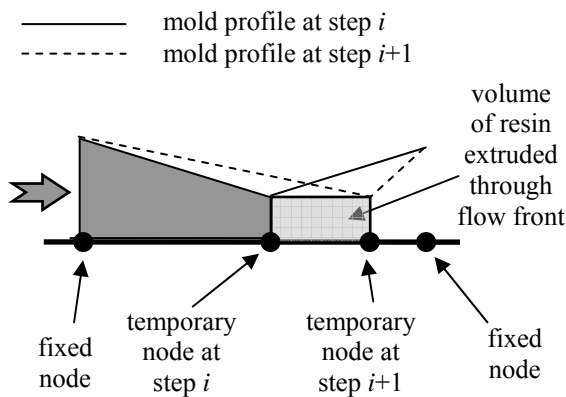


Fig. 2. profile changes at the flow front

The residual corresponding to the implicit Eqns. 12-13 is next calculated and an iterative improvement for the heights is obtained. The procedure is repeated until convergence is achieved. The time-step can be altered dynamically depending

on the number of Newton-Raphson iterations required for convergence. The temporary flow-front elements are discarded as filling proceeds (as elements completely fill) and new temporary nodes are generated.

### 3.3 Error Quantification

A Resin Discrepancy Percentage (RDP) was calculated to indicate the difference between the volume of resin which had entered the mold and the volume which was actually in the mold. The RDP provided an indication of simulation error, and fell consistently with mesh refinement. In all cases, the RDP was found to indicate more resin in the mold than there ought to be.

## 4 Results and Discussion

Simulations were run for a glass-fibre continuous filament mat (8 layers of CFM, density  $2.58 \text{ g/cm}^3$ , areal mass  $450 \text{ g/m}^2$ , diameter  $15 \mu\text{m}$ ), and the following data was used:

The Carman-Kozeny relation

$$K_{ij} = \frac{d^2 (1 - V_f)^3}{16k V_f^2} \quad (19)$$

was used for Eqn. 5 with  $d = 10^{-5}$ ,  $k = 3.125 \times 10^{-3}$ . The elastic law

$$\sigma_f = E \ln \left( \frac{h_0}{h} \right)^n \quad (20)$$

was used for Eqn. 7, where  $h_0$  is the initial thickness. For a dry perform,  $E = 125 \text{ kPa}$  and  $n = 5$ . For a wet perform,  $E = 55 \text{ kPa}$  and  $n = 6$ .

### 4.1 Thickness profiles

Figures 3 and 4 display thickness profiles for uni-directional filling of a  $0.5 \text{ m} \times 0.5 \text{ m}$  preform with constant (atmospheric) injection pressure. Satisfactory convergence was achieved with 50 element sub-divisions along the length of the mold. Fig. 3 displays profiles at 20s intervals for the standard Darcy law (SD) whilst Fig. 4 displays profiles at 3s intervals for the height-averaged law (AD).

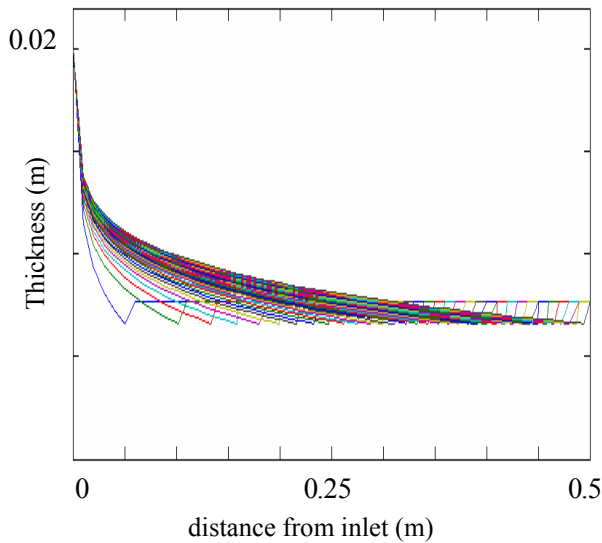


Fig. 3. Thickness profiles during filling (SD)

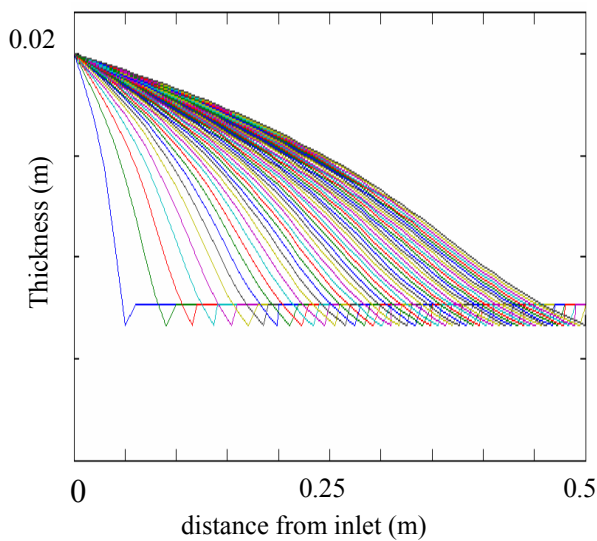


Fig. 4. Thickness profiles during filling (AD)

Note the pronounced swelling effect in the case of the thickness averaged Darcy's law. Eqns. 3 and 8 are, essentially, empirical laws, and which is the more appropriate can be determined only by carrying out suitable experiments and comparing with simulation results. Experimental data for thickness profiles in infusion processes (in the absence of distribution media) is scarce. The experimental data which is currently available to us lacks the required precision due to instrumentation inadequacies and can only be used in a cautious, qualitative, way. Nevertheless, the simulation results for thickness profiles do appear to mirror the trends

of the experimental data. Further experimental studies with a view to analyzing further the appropriateness of the AD model are underway at present.

Fig. 5 illustrates the changing thickness of the preform at a location 0.15m from the inlet. This typical profile shows the abrupt change from "dry" to "wet" as the flow-front passes and then the gradual increase in thickness due to increasing fluid pressure (and hence decreasing fibre stress).

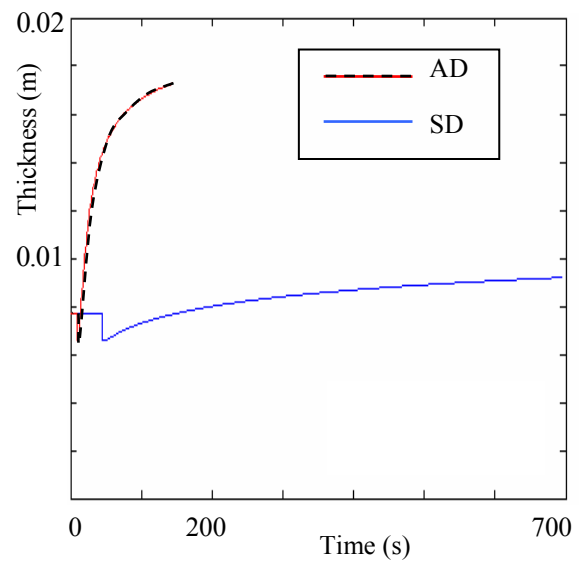


Fig. 5. Thickness profiles 0.15m from inlet

#### 4.2 Pressure Distributions

The pressure distributions at the end of filling are shown in Fig. 6. For the AD model, the pressure drops significantly near the flow front, producing a large negative pressure gradient and hence a large Darcy velocity. This results in the low fill-time seen in Fig. 5. In a substantial region near the inlet the pressure is close to the injection pressure and the pressure gradient is low. For the SD model, the gradient of the pressure distribution does not vary so much along the mould and is in fact quite similar to that predicted in constant-thickness RTM simulations.

Note that, due to the non-linear nature of the fibre stress-strain relation, small increments in fluid pressure when the fibre is close to its free/unstressed height (and so  $\sigma_f$  is large) result in much larger increments in fibre compression than when the fibre is already under some compression.

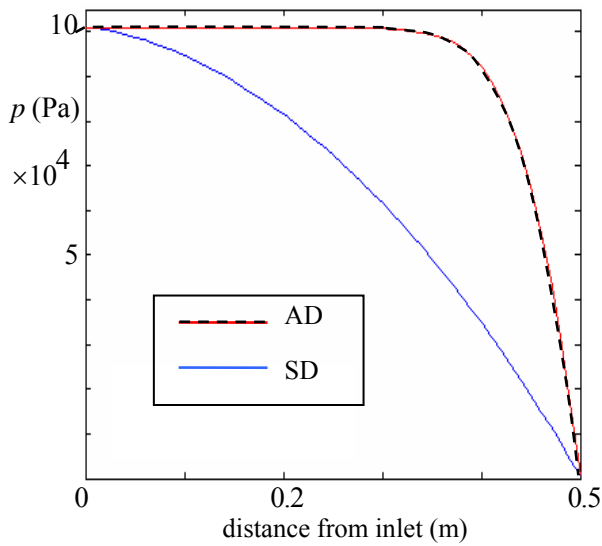


Fig. 6. Pressure distributions at completion of filling

### 4.3 Quasi-Static Approximation

A quasi-static approximation of the process can be made by taking  $\partial h / \partial t = 0$  in all expressions. The thickness profiles thus obtained are a very good approximation of those from the full transient simulation. This can be seen from Fig. 7 (in which the SD model is used).

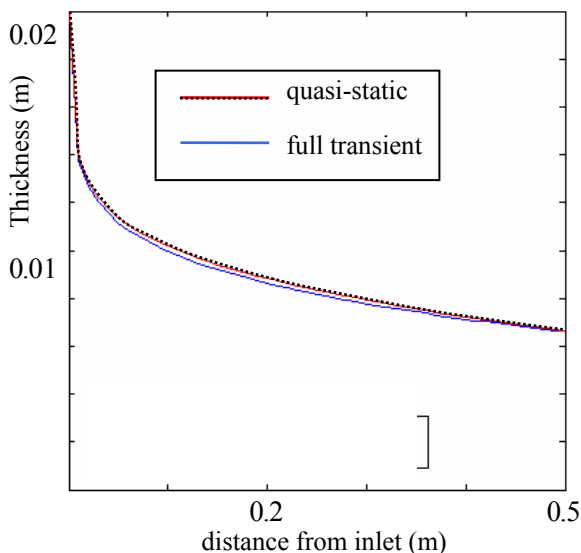


Fig. 7. Comparison of height profiles for full and quasi-static simulations (SD)

However, the predicted fill-times are very different: whereas the full solution predicts a fill-

time of 700 (SD) or 144 (AD) seconds (see Fig. 5), the quasi-static solution predicts a fill time of 570 (SD) or 68 (AD) seconds. Further, relatively high RDP values result from the quasi-static method. This suggests that the temporal height derivative is significant and, although the neglecting of it reduces the simulation time considerably, it cannot lightly be discarded.

## 5 Conclusions

In this study, the Resin Infusion process has been effectively simulated. Two models were used, one based on the conventional Darcy's Law (SD) and one based a height-averaged modified version of Darcy's Law (AD). Which of these models is more appropriate is still open to question – further experimental work is required.

The temporary node method used in the simulations replaces the conventional control volumes with the computational elements and uses a Taylor's series expansion in elements at the flow front to approximate the flow front fluxes. Elements at the flow front are allowed to expand as the resin saturates more of the fibre in the mould.

The temporal height derivative is important and cannot be neglected if one is interested in an accurate simulation. Neglecting this term to form the quasi-static forms of the full governing equations significantly increases the mass balance error and can greatly reduce the mold fill time.

## References

- [1] Šimáček P. and Advani S.G. "Desirable features in mold filling simulations for Liquid Composite Molding processes". *Polymer Composites*, Vol. 25, No. 4, pp 355-367, 2004
- [2] Deleglise M., Binetruy C. and Krawczak P. "Simulation of LCM processes involving induced or forced deformations", *Composites: Part A*, Vol. 37, pp 874-880, 2006.
- [3] Kelly P.A. and Jennings S. "Non-conforming elements for Liquid Composite Molding processes". *Proceedings of the 8<sup>th</sup> International Conference on Flow Processes in Composite Materials (FPCM8)*, Douai, France, pp 315-321, 2006.
- [4] Chou S-H. and Tang S. "Conservative P1 conforming and non-conforming Galerkin FEMs: effective flux evaluation via a non-mixed approach". *SIAM J. Numer. Anal.* Vol 38, pp 660-680, 2000.
- [5] Kang M.K. and Lee W.I. "A flow-front refinement technique for the numerical simulation of the resin-transfer molding process". *Comp. Sci. Tech.* Vol. 59, pp 1663-1674, 1999.